

Halo structure of ${}^6\text{He}$ from *ab initio* two-nucleon spatial correlations

Mengyao Huang,^{1,2} Tobias Frederico,³ Peng Yin,^{4,5,1}
Robert A. M. Basili,^{1,6} Patrick J. Fasano,^{7,1,8} and James P. Vary¹

¹*Department of Physics and Astronomy, Iowa State University, Ames, Iowa 50011, USA*

²*Lawrence Livermore National Laboratory, P.O. Box 808, L-414, Livermore, California 94551, USA*

³*Instituto Tecnológico de Aeronáutica, DCTA, 12228-900 São José dos Campos, Brazil*

⁴*College of Physics and Engineering, Henan University of Science and Technology, Luoyang 471023, China*

⁵*CAS Key Laboratory of High Precision Nuclear Spectroscopy,
Institute of Modern Physics, Chinese Academy of Sciences, Lanzhou 730000, China*

⁶*Department of Mathematics, Iowa State University, Ames, Iowa 50011, USA*

⁷*Department of Physics and Astronomy, University of Notre Dame, Notre Dame, Indiana 46556, USA*

⁸*NextSilicon Ltd., Minneapolis, Minnesota 55402-1572, USA*

We evaluate pairwise correlations using ground state wave functions for ${}^4\text{He}$ and ${}^6\text{He}$ obtained by *ab initio* no-core shell model (NCSM) calculations with the Daejeon16 nucleon-nucleon interaction plus Coulomb interaction, to characterize the structures of these two systems. We demonstrate that two-nucleon spatial correlations, specifically the pair-number operator r^0 and the square-separation operator r^2 projected on two-body spin S and isospin z -components encode important details of the halo structure of ${}^6\text{He}$. We also analyze the single-particle state occupancies and the two-body state occupancies for the ground state of ${}^4\text{He}$ and ${}^6\text{He}$. Our results indicate that the two valence neutrons in the ground state of ${}^6\text{He}$ dominantly form a spin-singlet configuration. The rms pair separations between core nucleons and halo neutrons of ${}^6\text{He}$ is about 80% larger than pair separations within the swollen and off-centered “ α core”. We show that this off-centering effect is primarily responsible for the observed increase in point-proton radius r_p in ${}^6\text{He}$ relative to ${}^4\text{He}$.

I. INTRODUCTION

Clustering phenomena in atomic nuclei reflect both the degrees of freedom of individual nucleons and collective structures within the nucleus. As a natural example, certain nuclei near the “drip lines” (where nucleons are nearly free to escape) are likely formed with a relatively stable core and a “halo” made of one or more nucleons loosely bound to the core [1–5].

Neutron halos have drawn significant attention since the 1980s when the surprisingly large interaction cross section of ${}^{11}\text{Li}$ compared with other Li isotopes was observed in radioactive ion beam (RIB) transmission experiments [6–8]. These nuclei also display a narrow core momentum distribution in peripheral breakup reactions [9, 10]. Strong electric dipole ($E1$) excitations at low excitation energies were observed in some of the halo nuclei, attributed to their weakly bound halo neutron(s) undergoing excitation to the continuum states [11–13]. Although there is no clear-cut distinction between halo and non-halo nuclei, halo nuclei are recognized by their shared characteristics. Nuclei with a neutron halo, for example, display a long tail in the neutron density distribution profile, and have small neutron separation energies for the halo neutron(s).

Over the years, many efforts have been made to extract the clustering information from *ab initio* calculations. The *ab initio* NCSM/RGM (no-core shell model/resonating group method) was used to perform calculations on a ${}^4\text{He}$ (ground state) + $n + n$ cluster basis, with results consistent with *ab initio* NCSM calculations without a cluster basis [14–16]. Cluster form factors were extracted [17], and further improvements have been

made to the work on three-cluster dynamics within the *ab initio* NCSM with continuum [16, 18]. The *ab initio* lattice approach implementing chiral effective field theory successfully modeled a 3- α structure for the Hoyle state of ${}^{12}\text{C}$ [19]. More recently, *ab initio* configuration interaction methods have revealed the important roles of α -clustering in light nuclei including details on the ground and Hoyle excited state of ${}^{12}\text{C}$ [20]. In addition, measures of entanglement of ${}^4\text{He}$ and ${}^6\text{He}$ nuclei were explored using *ab initio* nuclear many-body calculations [21], where a core-valence structure naturally emerges from the full no-core calculation of ${}^6\text{He}$ by analyzing common features of entanglement.

From a computational point of view, studying the clustering properties of nuclei could help us design improved basis functions and usefully subdivide the Hilbert space into regions of greater and lesser importance. Spatial information such as the average relative separations of nucleons in a system is key to characterizing the cluster wave functions. Accordingly, we examine the structure of a nucleus by *ab initio* calculations utilizing two-body correlations. Previously, one-body probabilities have been used in the *ab initio* NCSM [22] with great success in revealing information on the clustering of Li isotopes [23, 24]. Using two-body operators has the advantage of unfolding the detailed structure of the dominant configuration and displaying the differences in the nucleon-nucleon correlations among pairs of nucleons in specific two-body configurations. Besides the most commonly used spatial parameters (the rms radii), we explore the two-body spatial moments r^0 and r^2 —called the pair-number operator and the square-separation operator, respectively—projected on each two-body state

sector.

We choose ${}^6\text{He}$ as a test case in this new method owing to its relative simplicity. It is the lightest Borromean halo nucleus which means that neither of the two-component substructures, n - n or n - α in the $\alpha+n+n$ system, is bound when one removes the third component. In this case, the one-body density profile cannot fully reveal the geometrical structure of the $2n$ -halo, while two-body correlations can probe the relative distance between the two valence neutrons compared with the relative distances of the other pairs of nucleons. Our primary focus is to introduce our method and demonstrate its application to ${}^6\text{He}$ in advance of achieving fully converged *ab initio* NCSM results for the two-body correlations that we develop and employ. We defer the development of suitable extrapolation methods for these two-body correlations to a later project.

In the following sections, we first introduce the coordinate space two-body operators we will use (Sec. II) and the approach to solving the quantum many-body problem (Sec. III). We then present and discuss the calculated expectation values of these two-body operators and how they relate to the halo structure of ${}^6\text{He}$ (Sec. IV).

II. CONSTRUCTING TWO-BODY OPERATORS IN COUPLED- J BASIS

To carry out a quantitative analysis of the distributions of nucleons and pairs of nucleons within a nucleus, one needs appropriate operators that sample these quantities. For this purpose, we will define two-body operators whose expectation values within the nuclear ground state will inform our detailed analysis of how nucleons are arranged in coordinate space on average. The standard basis we use is the spherical single-particle basis, which is denoted by its quantum numbers, including radial quantum number n , orbital angular momentum l , spin s , total angular momentum j , total angular momentum projection m_j , isospin t and isospin z -projection t_z . We can use the short-hand notation

$$\alpha = \{n_\alpha, l_\alpha, \frac{1}{2}, j_\alpha, m_{j_\alpha}, \frac{1}{2}, t_{z\alpha}\}, \quad (1)$$

where the first “ $1/2$ ” is for nucleon spin s and the second “ $1/2$ ” is for nucleon isospin t .

To compute matrix elements of two-body operators in a basis with “good” two-body total angular momentum J , we work in terms of the spherical tensor coupled product [25], e.g.,

$$\{a_\alpha^\dagger a_\beta^\dagger\}_{J,M} = \sum_{m_{j_\alpha}, m_{j_\beta}} C_{m_{j_\alpha} m_{j_\beta}}^{j_\alpha j_\beta J} a_\alpha^\dagger a_\beta^\dagger, \quad (2)$$

where M is the z -projection of J . $C_{m_{j_\alpha} m_{j_\beta}}^{j_\alpha j_\beta J}$ are the Clebsch-Gordan coefficients. To keep notation compact, we suppress the label M and introduce the resulting coupled- J basis states,

$$|\alpha\beta; J\rangle = \{a_\alpha^\dagger a_\beta^\dagger\}_{J|0}. \quad (3)$$

When calculating observables represented by one-body and two-body operators, one may compute the corresponding density matrices between the desired initial and final states, from which all matrix elements can subsequently be extracted via weighted summation. The two-body density matrix in the coupled- J basis is

$$\begin{aligned} \rho_{\{\alpha\beta\}_{J'}\{\gamma\delta\}_J} &= \langle \Phi'_A | \{a_\alpha^\dagger a_\beta^\dagger\}_{J'} \{a_\delta a_\gamma\}_J | \Phi_A \rangle \\ &= \sum_{m_{j_\alpha}, m_{j_\beta}} C_{m_{j_\alpha} m_{j_\beta}}^{j_\alpha j_\beta J'} \sum_{m_{j_\gamma}, m_{j_\delta}} C_{m_{j_\gamma} m_{j_\delta}}^{j_\gamma j_\delta J} \rho_{\alpha\beta\gamma\delta} \end{aligned} \quad (4)$$

where the $\rho_{\alpha\beta\gamma\delta}$ are two-body density matrix elements in the uncoupled single-particle representation.

The expectation value of a two-body operator in a system of nucleons expressed in the coupled- J basis can thus be written as

$$\langle \Phi'_A | \mathcal{O}_{2B} | \Phi_A \rangle = \sum_{\{\alpha\beta\}_{J'}\{\gamma\delta\}_J} \rho_{\{\alpha\beta\}_{J'}\{\gamma\delta\}_J} \langle \alpha\beta; J' | \mathcal{O} | \gamma\delta; J \rangle, \quad (5)$$

where \mathcal{O} is redefined as an operator acting on the coupled- J basis.

A rotationally invariant two-body operator $\mathcal{O}(r)$ suitable to our purpose, with a given two-body spin S and a given pair of isospin z -projections $\{t_{z\alpha}, t_{z\beta}\}$, acting on the coupled- J basis yields the matrix elements (derived in Appendix A)

$$\begin{aligned} \langle \alpha\beta; J' M' | \mathcal{O}(r) | S, t_{z\alpha}, t_{z\beta} | \gamma\delta; JM \rangle &= \delta_{t_{z\alpha}, t_{z\gamma}} \delta_{t_{z\beta}, t_{z\delta}} \delta_{J' J} \delta_{M' M} g(t_{z\alpha}, t_{z\beta})_{t_{z\alpha} \leq t_{z\beta}} \\ &\times (2S+1) \sqrt{(2j_\alpha+1)(2j_\beta+1)(2j_\gamma+1)(2j_\delta+1)} \\ &\times \sum_L (2L+1) \begin{Bmatrix} l_\alpha & l_\beta & L \\ 1/2 & 1/2 & S \\ j_\alpha & j_\beta & J \end{Bmatrix} \begin{Bmatrix} l_\gamma & l_\delta & L \\ 1/2 & 1/2 & S \\ j_\gamma & j_\delta & J \end{Bmatrix} \langle n_\alpha l_\alpha n_\beta l_\beta L | \mathcal{O}(r) | n_\gamma l_\gamma n_\delta l_\delta L \rangle, \end{aligned} \quad (6)$$

where L is the two-body total orbital angular momentum

and we define $g(t_{z\alpha}, t_{z\beta})_{t_{z\alpha} \leq t_{z\beta}} \equiv \delta_{t_{z\alpha}, t_{z\alpha}} \delta_{t_{z\beta}, t_{z\beta}} + (1 -$

$\delta_{t_{z\alpha}, t_{z\beta}} \delta_{t_{z\alpha}, t_{z\beta}} \delta_{t_{z\beta}, t_{z\alpha}}$ which has the property:

$$g(t_{z\alpha}, t_{z\beta})_{t_{z\alpha} \leq t_{z\beta}} = \begin{cases} 1, & \text{if } t_{z\alpha} = t_{z\alpha} \text{ and } t_{z\beta} = t_{z\beta} \\ 1, & \text{if } t_{z\alpha} = t_{z\beta} \text{ and } t_{z\beta} = t_{z\alpha} \\ 1, & \text{if } t_{z\alpha} = t_{z\beta} = t_{z\alpha} = t_{z\beta} \\ 0, & \text{otherwise} \end{cases}. \quad (7)$$

This function ensures that any pair of isospin z -projections $\{t_{z\alpha}, t_{z\beta}\}$ has at most one way to match the given values $\{t_{z\alpha}, t_{z\beta}\}$ with $t_{z\alpha} \leq t_{z\beta}$, as well as the exchange symmetry of $t_{z\alpha}$ and $t_{z\beta}$.

We then introduce a notation to describe an operator acting within a system of nucleons (similar to the $U[u]$ and $V[v]$ operators defined in Ref. [26])—the subscript A , which means that we apply the operator on all nucleon pairs in the A -body space, i.e. $\mathcal{O}_A \equiv \sum_{i < j}^A \mathcal{O}$ for two-body operators and $\mathcal{O}_A \equiv \sum_i^A \mathcal{O}$ for one-body operators. Thus, the expectation value of $\mathcal{O}(r)[S, t_{z\alpha}, t_{z\beta}]$ in the A -body space is

$$\begin{aligned} \langle \mathcal{O}(r)_A [S, t_{z\alpha}, t_{z\beta}] \rangle &= \langle \sum_{i < j}^A \mathcal{O}(r_{ij}) [S, t_{z\alpha}, t_{z\beta}] \rangle \\ &= \sum_{\{\alpha\beta\}_J, \{\gamma\delta\}_J} \rho_{\{\alpha\beta\}_J, \{\gamma\delta\}_J} \langle \alpha\beta; J' | \mathcal{O}(r) [S, t_{z\alpha}, t_{z\beta}] | \gamma\delta; J \rangle, \end{aligned} \quad (8)$$

where $r_{ij} = |\vec{r}_i - \vec{r}_j|$ is the relative distance between the i th and j th nucleon, and $i, j = 1, 2, \dots, A$. α and γ (β and δ) denote the initial and final single-particle states of the i th (j th) nucleon, respectively. In the following, the subscript A is conveniently omitted when referring to the expectation values of the operator (denoted by a bracket directly around the operator), i.e., $\langle \mathcal{O} \rangle \equiv \langle \mathcal{O}_A \rangle$.

In Sec. II A and Sec. II B, we will define the pair-number operator and the square-separation operator with given S and isospin z -projections which determine the nucleon species (proton-proton, neutron-proton and neutron-neutron, indicated as pp , pn , and nn , respectively). Combining them will provide information on mean square separations of a pp , pn or nn pair of nucleons with a given two-body spin S , which will be illustrated in Sec. IV C.

A. The pair-number operator

The pair-number operator r^0 for a given two-body spin S and a fixed pair of values of the isospin z -projections is $r^0[S, t_{z\alpha}, t_{z\beta}] \equiv P_S P_{t_{z\alpha}, t_{z\beta}}$. When applied to the A -nucleon space, its expectation value $\langle r^0[S, t_{z\alpha}, t_{z\beta}] \rangle$ is

$$\sum_{\{\alpha\beta\}_J, \{\gamma\delta\}_J} \rho_{\{\alpha\beta\}_J, \{\gamma\delta\}_J} \langle \alpha\beta; J | P_S P_{t_{z\alpha}, t_{z\beta}} | \gamma\delta; J \rangle. \quad (9)$$

$\langle r^0[t_{z\alpha}, t_{z\beta}] \rangle$ is obtained by summing over S in the ex-

pression above,

$$\begin{aligned} &\sum_{\{\alpha\beta\}_J, \{\gamma\delta\}_J} \rho_{\{\alpha\beta\}_J, \{\gamma\delta\}_J} \langle \alpha\beta; J | P_{t_{z\alpha}, t_{z\beta}} | \gamma\delta; J \rangle \\ &= \sum_{\{\alpha\beta\}_J} \rho_{\{\alpha\beta\}_J, \{\alpha\beta\}_J} g(t_{z\alpha}, t_{z\beta})_{t_{z\alpha} \leq t_{z\beta}}, \end{aligned} \quad (10)$$

which is an integer according to Eq. (7) and Eq. (4), meaning the number of pairs with a given pair of isospin z -projections (however, $\langle r^0[S, t_{z\alpha}, t_{z\beta}] \rangle$ is generally not an integer). It will become clearer when we present the calculation results in Sec. IV B.

Taking into account all possible isospin z -projections,

$$\langle r^0 \rangle = \sum_{t_{z\alpha} \leq t_{z\beta}} \langle r^0[t_{z\alpha}, t_{z\beta}] \rangle = \sum_{i < j}^A 1 = \frac{A(A-1)}{2}, \quad (11)$$

which is the total number of pairs of nucleons in an A -nucleon system. The value of 1 inside the summation of the second line of Eq. (11) comes from that any pair of nucleons' isospin z -projection values automatically falls into one of the first three cases in Eq. (7) when there is no restriction on the values of isospin z -projections.

B. The square-separation operator

The expectation value of the square-separation operator r^2 in the two-body space describes the relative distance squared for a pair of nucleons. The square-separation operator for a given two-body spin S and a fixed pair of values of isospin z -projections is defined as $r^2[S, t_{z\alpha}, t_{z\beta}] \equiv r^2 P_S P_{t_{z\alpha}, t_{z\beta}}$. Its expectation value in an A -body space $\langle r^2[S, t_{z\alpha}, t_{z\beta}] \rangle$ is

$$\sum_{\{\alpha\beta\}_J, \{\gamma\delta\}_J} \rho_{\{\alpha\beta\}_J, \{\gamma\delta\}_J} \langle \alpha\beta; J | r^2 P_S P_{t_{z\alpha}, t_{z\beta}} | \gamma\delta; J \rangle. \quad (12)$$

$\langle r^2[t_{z\alpha}, t_{z\beta}] \rangle$ represents the expectation value for restrictions on isospin z -projections only, which is

$$\sum_{\{\alpha\beta\}_J, \{\gamma\delta\}_J} \rho_{\{\alpha\beta\}_J, \{\gamma\delta\}_J} \langle \alpha\beta; J | r^2 | \gamma\delta; J \rangle g(t_{z\alpha}, t_{z\beta})_{t_{z\alpha} \leq t_{z\beta}}. \quad (13)$$

C. Relation to the rms radii

The square of the nuclear matter rms radius r_m with center-of-mass coordinates $\vec{R}_{\text{cm}} = (\sum_i^A \vec{r}_i)/A$ is

$$r_m^2 \equiv \frac{1}{A} \sum_i^A (\vec{r}_i - \vec{R}_{\text{cm}})^2 = \frac{1}{A^2} \sum_{i < j}^A (\vec{r}_i - \vec{r}_j)^2 = \frac{r_A^2}{A^2}, \quad (14)$$

where r_A^2 is the square-separation operator in the A -nucleon space. Projecting r_A^2 on different isospin z -components and scaled by $1/A^2$ yields the point-proton

and point-neutron rms radii r_p and r_n [27]. This means that the convergence behavior of the results from the r^2 operator is similar to that of rms radii. Thus, in Sec. IV A, we use calculated rms radii to determine the suitable parameters for our calculation of r^0 and r^2 .

III. AB INITIO NCSM CALCULATION

We obtain the matrix elements of operators r^0 and r^2 in the harmonic oscillator (HO) relative motion basis (Appendix B), and transform them to two-body matrix elements in the single-particle basis by the Moshinsky transformation sketched in Appendix C. The resulting two-body matrix elements are then employed to calculate expectation values using many-body NCSM wavefunctions. We adopt the Daejeon16 two-nucleon (NN) interaction [28] as well as Coulomb interaction in our *ab initio* NCSM calculations using the MFDn code [29, 30]. The Daejeon16 interaction is obtained by softening the chiral effective field theory (χ EFT) based Idaho next-to-next-to-next-to-leading order (N3LO) NN interaction using the similarity renormalization group (SRG) method [31, 32]. Five significant figures are preserved throughout our calculation process.

The calculated rms radii for ^4He and ^6He are presented in Sec. IV A. They provide a handle for choosing the many-nucleon basis space cutoff N_{max} and HO energy spacing $\hbar\Omega$ to minimize the basis truncation error of the expectation values for the r^0 and r^2 operators with limited computational resources. We then compare these rms radii with the experimental values to underpin the utility of the calculations and inform the uncertainties arising from our NCSM calculations. Later, we present in Sec. IV B the results of the r^0 operator and analyze the results in detail with the help of the occupation distribution of single-particle states and two-body states which also result from our calculations. We show how the r^0 and r^2 operators provide insight to the halo structure of ^6He in Sec. IV B and Sec. IV C.

IV. RESULTS AND ANALYSIS

A. The rms radii

To determine N_{max} and $\hbar\Omega$ values that limit our truncation error, we calculate r_p , r_n and r_m on a grid of N_{max} from 6 to 18 with a step size of 2, and $\hbar\Omega$ from 10 to 30 MeV, sampled every 2.5 MeV with additional points at 8 and 9 MeV for $N_{\text{max}} \leq 16$. The results for ^4He and ^6He are shown in Fig. 1.

We find the range $\hbar\Omega = 10$ MeV to 27.5 MeV provides an approximate N_{max} independence for the point-nucleon rms radii for ^4He . This is evident in Fig. 2 through the very small differences (on the order of 10^{-4} fm) in the point-nucleon rms radii between $N_{\text{max}} = 16$ and $N_{\text{max}} = 18$ over this range of $\hbar\Omega$ over this range of

$\hbar\Omega$. For ^6He , however, the differences between neighboring N_{max} (denoted as Δr) decrease with increasing N_{max} but do not display a very good convergence pattern as shown in both Fig. 1 and Fig. 2. With an emphasis on minimizing Δr for ^6He while achieving a reasonable $\hbar\Omega$ -independence for it, we adopt $\hbar\Omega = 10$ MeV. This choice also provides good convergence of Δr for ^4He . Finally, we adopt $N_{\text{max}} = 16$ since it is sufficient for our demonstration purposes of calculating our suite of characteristic matrix elements with limited computational resources.

We show in Table I r_p , r_n and r_m for both ^4He and ^6He with $N_{\text{max}} = 16$ and $\hbar\Omega = 10$ MeV. We note that r_n is about 39% (0.7 fm) larger than r_p for ^6He . On the other hand, r_p increases by 25% from ^4He (1.515 fm) to ^6He (1.889 fm). As we will show, this increase in r_p may be understood as arising from the motion of the charged “ α core” around the common center of mass, as well as from contributions from swelling of the “ α core” [33]. Specifically, we show in Sec. IV C, that the rms separations indicate the swelling effect only contributes a few percent increase to r_p while the center-of-mass deviation effect is prominent in ^6He .

To analyze the uncertainties resulting from the $N_{\text{max}} = 16$ truncation and examine the consistency with the experimental values, we present r^* and r^{exp} values in Table I, explained as follows. r_p^* , r_n^* and r_m^* are those obtained with $N_{\text{max}} = 18$ and $\hbar\Omega$ corresponding to the minimum gap Δr between $N_{\text{max}} = 18$ and $N_{\text{max}} = 16$ results (For ^4He , $\hbar\Omega = 15$ MeV for $r_{p/m}^*$ and $\hbar\Omega = 17.5$ MeV for r_n^* ; For ^6He , $\hbar\Omega = 10$ MeV). Comparing r and r^* values gives an estimate of the magnitude of the basis cutoff uncertainties: For ^4He , the differences appear in the third decimal digit; For ^6He , the differences show up in the second decimal digit. The experimental point-nucleon rms radii $r_{p/n/m}^{\text{exp}}$ are indicated in the last column in Table I. r_p^{exp} is calculated using $r_p^2 = r_c^2 - R_p^2 - 3/(4M_p^2) - (N/Z)R_n^2 - r_{so}^2$, where the nucleus rms charge radius r_c can be measured from laser spectroscopy or scattering experiments, the Darwin-Foldy term $3/(4M_p^2) = 0.033 \text{ fm}^2$ [36] and the neutron mean square charge radius $R_n^2 = -0.1161(22)$ [36]. The relativistic correction due to spin-orbit interaction $r_{so}^2 = 0$ for ^4He and -0.08 fm^2 for ^6He [37]. The latest recommended value of $R_p = 0.84075(64)$ [38]. r_m^{exp} in Table I is obtained from the interaction cross sections of elastic scattering [33], while r_n^{exp} is computed from the universal relation $Ar_m^2 = Zr_p^2 + Nr_n^2$. The experimental ranges in Table I are visualized in Fig. 1 as color bands. Due to the large experimental uncertainties, $r_{m/n}^*$ remains consistent with $r_{m/n}^{\text{exp}}$ even without full convergence. On the other hand, the fully converged r_p^* for ^4He exceeds the upper edge of the experimental values by 0.02 fm, which is mainly due to the properties of the Daejeon16 potential [39]. The non-converged r_p^* for ^6He is 0.03 fm smaller than the lower edge of the experimental values and it has a favorable trend with larger N_{max} . In summary, comparing r with r^* , we estimate that the truncation error

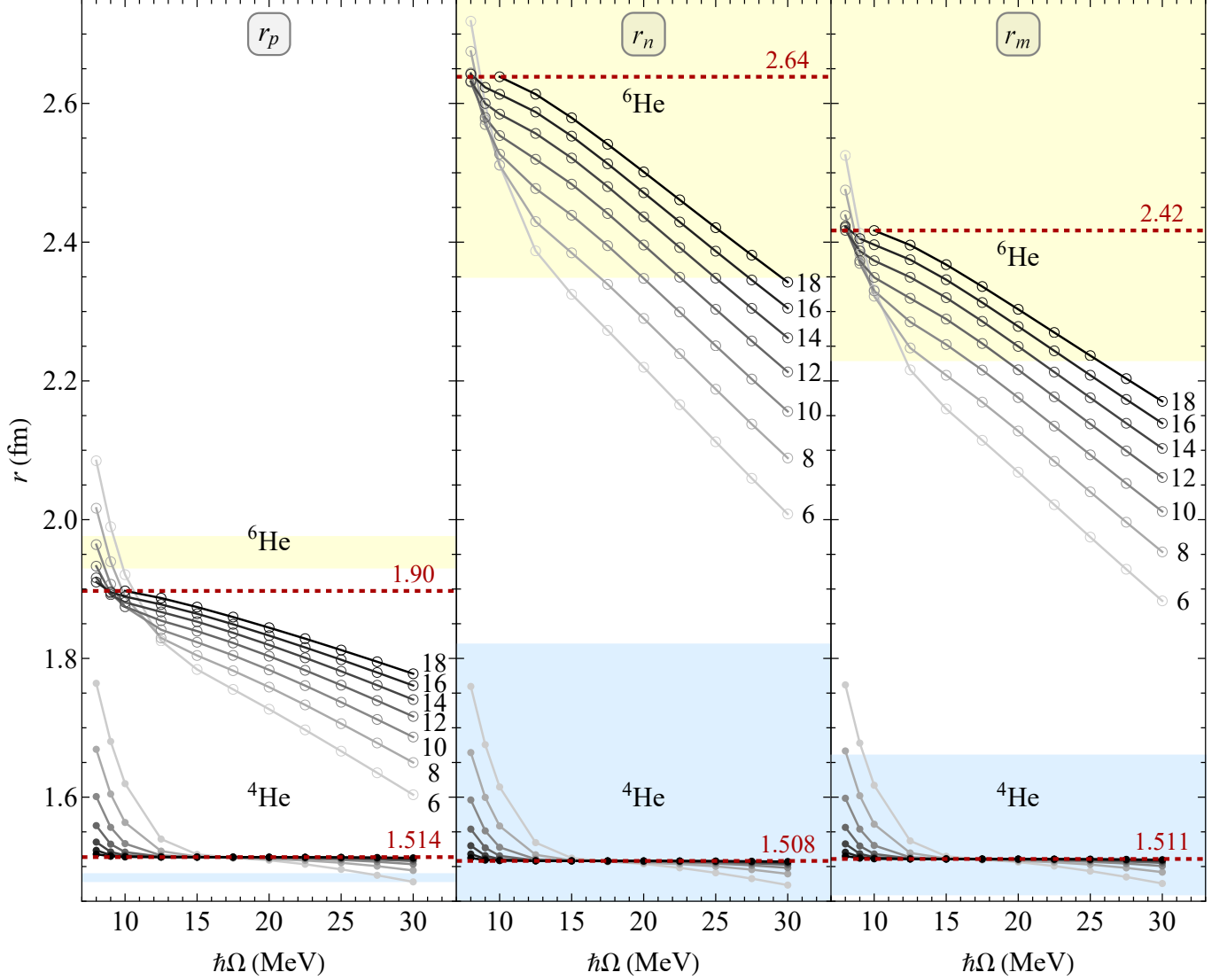


FIG. 1. r_p , r_n and r_m of ${}^4\text{He}$ (${}^6\text{He}$) with the Daejeon16 interaction plus Coulomb potential, calculated using *ab initio* NCSM. Results for ${}^4\text{He}$ (${}^6\text{He}$) are represented by filled (open) circles, which are connected by straight lines for the same N_{max} , with darker lines for higher N_{max} (N_{max} values are labeled on the right of the ${}^6\text{He}$ results). The horizontal red dashed lines indicate $r_{p/n/m}^*$ of ${}^4\text{He}$ (${}^6\text{He}$) for $N_{\text{max}} = 18$ with $\hbar\Omega$ determined by the minimum gap between $N_{\text{max}} = 18$ and $N_{\text{max}} = 16$ results. The experimental ranges are indicated by blue (for ${}^4\text{He}$) and yellow (for ${}^6\text{He}$) bands.

TABLE I. $r_{p/n/m}$ [fm] for ${}^4\text{He}$ and ${}^6\text{He}$ with $N_{\text{max}} = 16$ and $\hbar\Omega = 10$ MeV. $r_{p/n/m}^*$ [fm] is for $N_{\text{max}} = 18$ with $\hbar\Omega$ corresponding to the minimum gap between $N_{\text{max}} = 18$ and $N_{\text{max}} = 16$ results, serving as a reference for the uncertainty owing to the N_{max} truncation. The experimental values $r_{p/n/m}^{\text{exp}}$ [fm] are reported, where r_p^{exp} and r_m^{exp} are separately measurable, while r_n^{exp} is obtained using the relation $A r_m^2 = Z r_p^2 + N r_n^2$.

x	${}^4\text{He}$			${}^6\text{He}$		
	r_x	r_x^*	r_x^{exp}	r_x	r_x^*	r_x^{exp}
p	1.5145	1.5136	1.484(5) [34]	1.8891	1.8973	1.953(22) [35]
n	1.5091	1.5081	1.43–1.82	2.6132	2.6384	2.35–3.08
m	1.5118	1.5109	1.46–1.66 [33]	2.3963	2.4168	2.23–2.75 [33]

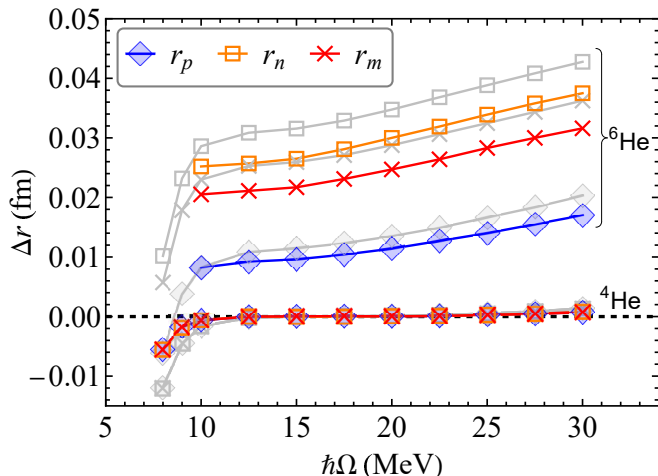


FIG. 2. The difference in $r_{p/n/m}$ between consecutive N_{\max} values: $N_{\max} = 18$ values minus $N_{\max} = 16$ values (color) and $N_{\max} = 16$ values minus $N_{\max} = 14$ values (gray). The absolute value of the difference $|\Delta r|$ serves as an indicator of the basis truncation uncertainty of $r_{p/n/m}$ at $N_{\max} = 16$.

is 0.001 fm (0.03 fm) for ${}^4\text{He}$ (${}^6\text{He}$). Comparing r^* with r^{exp} , we estimate that the systematic error (due to the potential) is 0.02 fm.

We continue with $N_{\max} = 16$ and $\hbar\Omega = 10$ MeV to calculate the expectation values for the r^0 and r^2 operators. We present six (five) decimal digits for the results of $\langle r^0[S, t_{za}, t_{zb}] \rangle$ ($\langle r^2[S, t_{za}, t_{zb}] \rangle$) to prevent losing significant digits in later calculations.

B. The expectation values of the r^0 operator

$\langle r^0[S, t_{za}, t_{zb}] \rangle$ provides the probability of finding a pair of nucleons with given S and $\{t_{za}, t_{zb}\}$. The results of $\langle r^0[S, t_{za}, t_{zb}] \rangle$ for both values of S and for all the $\{t_{za}, t_{zb}\}$ combinations are presented in Table II.

TABLE II. $\langle r^0[S, t_{za}, t_{zb}] \rangle$ calculated to five significant digits (denoted as “calc.”), with trailing digits grayed out. The naive expected value (denoted as “naive”) of each calculated result, based on occupying only the lowest available states in a HO basis, is listed for comparison as discussed in the text.

	S	${}^4\text{He}$		${}^6\text{He}$	
		naive	calc.	naive	calc.
pp	0	1	0.976772	1	0.967578
pp	1	0	0.023228	0	0.032422
pn	0	1	0.979111	2	1.977430
pn	1	3	3.020890	6	6.022570
nn	0	1	0.976774	3	2.865420
nn	1	0	0.023226	3	3.134580
all		6	6.000001	15	15.00000

nucleon	${}^4\text{He}$	${}^6\text{He}$
p	2	2
n	2	$\frac{n^\alpha}{n^h}$ 2
all	4	6

(a)

nucleons	${}^4\text{He}$	${}^6\text{He}$
pp	1	1
pn	4	$\frac{pn^\alpha}{pn^h}$ 4
nn	1	$\frac{n^\alpha n^\alpha}{n^h n^h}$ 4
all	6	15

(b)

TABLE III. Single-particle HO occupancies using lowest Pauli-allowed states (a) and resulting two-body matrix elements of r^0 (b) for ${}^4\text{He}$ and ${}^6\text{He}$ divided into charge-dependent categories. In ${}^6\text{He}$ we further divide the contributions into “ α core” (n^α) and “halo” (n^h) contributions.

First, we perform a sanity check for the sum of $\langle r^0[S, t_{za}, t_{zb}] \rangle$ over all $\{S, t_{za}, t_{zb}\}$ combinations for ${}^4\text{He}$ and ${}^6\text{He}$ (see Table II) to confirm that they are equal to the total number of nucleon pairs $A(A-1)/2$ for each nucleus as indicated by Eq. (11). We note that although the calculated $\langle r^0[S, t_{za}, t_{zb}] \rangle$ are not integers, a sum of $\langle r^0[S, t_{za}, t_{zb}] \rangle$ over two-body spin S equals the number of pairs with given $\{t_{za}, t_{zb}\}$ in ${}^4\text{He}$ and ${}^6\text{He}$, as suggested in Eq. (10). For example, $\langle r^0[0, 1/2, 1/2] \rangle_{{}^4\text{He}} + \langle r^0[1, 1/2, 1/2] \rangle_{{}^4\text{He}} = 0.976772 + 0.023228 = 1.000000 = \langle r^0[pp] \rangle_{{}^4\text{He}}$, recovering an integer within 5 significant digits.

${}^4\text{He}$ results are very close to integers and to naive expectations. We expect and find that both pp and nn in the ground state of ${}^4\text{He}$ are dominantly spin-singlet, because this is the only $l=0$ basis state (s -state) respecting the overall antisymmetrization for exchanging of two isospin-symmetric fermions, i.e. $(-1)^{l+S+T} = -1$, where l , S and T are the two-body orbital angular momentum in the two-body relative frame (see Appendix C), two-body spin and two-body isospin, respectively. One may also expect, as we indeed find, a small but non-zero portion of spin-triplet states (0.023228 for pp $S=1$ and 0.023226 for nn $S=1$) arising from partial wave contributions with higher values of l . The added Coulomb potential makes the isospin symmetry only approximate in our calculations (note that we assume equal mass for p and n , which is taken as the average mass of these nucleons; the Daejeon16 interaction is charge-independent), which contributes to the small difference between pp and nn expectation values for ${}^4\text{He}$.

For pn of ${}^4\text{He}$ in Table II, the result for spin-triplet is approximately triple the result for spin-singlet for the reason explained below. For the spin-independent parts of the NN interactions, singlet and triplet two-body spin states have the same energy in the same HO wave function of relative motion (labeled by n and l for two-body central potentials)—there is no preference among the allowed two-body spin configurations $\uparrow\uparrow$ (triplet), $\uparrow\downarrow$

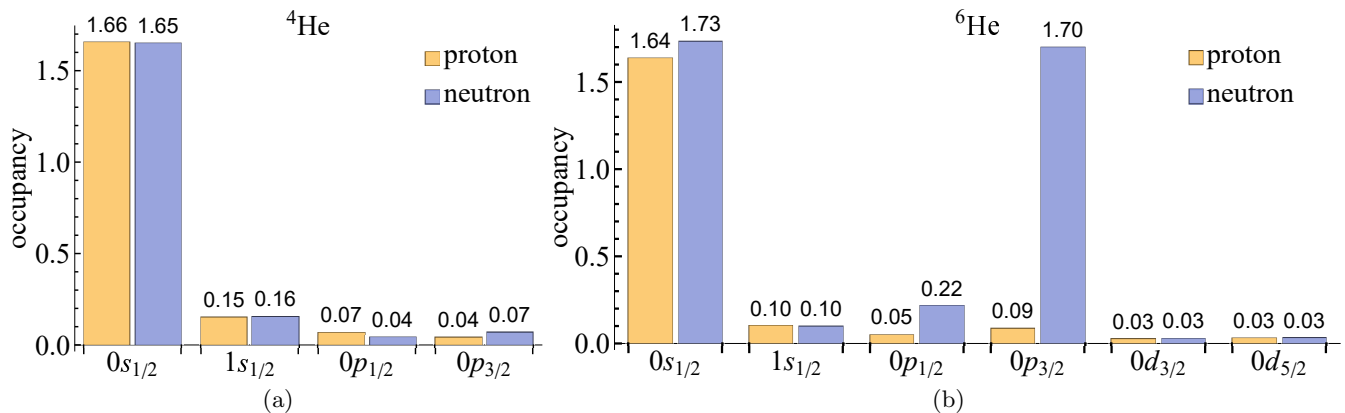


FIG. 3. Occupancy of protons and neutrons in HO single-particle states for the ground state of ^4He (a) and ^6He (b), with $N_{\text{max}} = 16$ and $\hbar\Omega = 10$ MeV. The HO single-particle state occupancies that are major contributors are shown and aggregate to more than 90% of the proton number or neutron number of each nucleus.

(triplet), $\uparrow\downarrow + \downarrow\uparrow$ (triplet) and $\uparrow\downarrow - \downarrow\uparrow$ (singlet). As a result, the ratio of the probability of triplet to singlet two-body spin states for the ground state of ^4He pn is approximately 3:1. Upon considering the spin-dependent part of the NN potential, e.g., $S_p S_n$ coupling in the s -state, which can be usefully written as $V_{\text{spin}} = \hbar^{-2} V_1(r) \vec{S}_p \cdot \vec{S}_n$ [40], the probability of finding a pair of pn in one of the triplet states will be slightly higher than in the singlet state if $V_1(r)$ is effectively attractive (thus negative), as in deuterium. This assessment takes into account $\langle \vec{S}_p \cdot \vec{S}_n \rangle = +\hbar^2/4$ for triplet states and $-\hbar^2/4$ for singlet states. These conditions are met, as can be seen in the calculated pn results of ^4He in Table II.

To pave the way for detailed inspection of the $\langle r^0[S, t_{za}, t_{zb}] \rangle$ results conveyed in Table II, we consider the NCSM results for the occupancies of the lowest HO single-particle states in ^4He and ^6He as shown in Fig. 3. The dominant occupancies are seen to be near the limits of a naive shell model picture where the lowest Pauli-allowed states are occupied assuming the traditional spin-orbit splitting of p -shell states. In particular, Fig. 3 shows that the lowest HO s -state contains well-above 80% of the maximum occupation number of two for protons and neutrons in both ^4He and ^6He . In addition, for ^6He , we obtain a similar occupation for neutrons in the HO $0p_{3/2}$ orbit. With more than 80% of nucleons occupying the lowest Pauli-allowed HO states, we adopt the naive shell model picture provides as a starting point for investigating matrix elements of two-nucleon operators.

In Table III we present the extreme values for HO single particle state occupancies (part (a)) and the pair identity operator r^0 (part(b)) as a function of charge for ^4He and ^6He . For neutrons in ^6He , we further divide their contributions into the s -state components which we call the “ α core” neutrons (denoted as n^α) and the p -state components or “halo neutrons” (denoted as n^h). We regard n^α and n^h as two categories of neutron, they then form two categories for pn (pn^α and pn^h) and three categories for nn ($n^\alpha n^\alpha$, $n^\alpha n^h$ and $n^h n^h$), as shown in Ta-

ble III(b).

The analyses above helps to see why the calculated $\langle r^0[S, t_{za}, t_{zb}] \rangle$ of ^6He in Table II are also consistent with naive expectations. In particular, since there is only a small change of proton occupancy from ^4He to ^6He , we expect and find that pp -pair occupancy should remain largely in the spin-singlet state. Correspondingly, pn^α has similar correlations as pn of ^4He . In other words, it is thrice as likely to find a spin-triplet state than to find a spin-singlet state in pn^α .

We speculate that the ratio of spin-triplet to spin-singlet state occupancies in pn^h will be close to those of pn^α . The reason is as follows. First, for the ^6He neutrons, the $0s_{1/2}$ and $0p_{3/2}$ occupancies are large and approximately equal. Second, the condition that the total angular momentum is zero suggests that the n^α and n^h have the same spin distributions. Therefore, pn^h will likely mimic pn^α with nearly no preference among the four two-body spin states: $\uparrow\uparrow$ (triplet), $\downarrow\downarrow$ (triplet), $\uparrow\downarrow + \downarrow\uparrow$ (triplet) and $\uparrow\downarrow - \downarrow\uparrow$ (singlet). For the same reason, except p replaced by n^α in pn^h , the two-body spin states in $n^\alpha n^h$ will mimic those in pn^α , i.e., three $n^\alpha n^h$ pairs in spin-triplet states and one $n^\alpha n^h$ pair in a spin-singlet state. To a lesser extent, we also expect both $n^\alpha n^\alpha$ and $n^h n^h$ to be dominantly in spin-singlet states, assuming that the correlations of neutrons within each shell are stronger than correlations of neutrons across different shells. This assumption seems to be approximately true, because the difference between the expected and calculated $\langle r^0[S, t_{za}, t_{zb}] \rangle$ for ^6He nn pairs in Table II is only 0.13.

We now address the role of N_{max} truncation. The maximum difference in $\langle r^0[S, t_{za}, t_{zb}] \rangle$ between $N_{\text{max}} = 16$ and $N_{\text{max}} = 14$ is 10^{-4} for ^6He pp/pn pairs and 5×10^{-4} for ^6He nn pairs. These are meaningful differences since the MFDn calculation preserves 5 significant digits. On the other hand, for ^4He , the maximum difference in $\langle r^0[S, t_{za}, t_{zb}] \rangle$ between $N_{\text{max}} = 16$ and $N_{\text{max}} = 14$ is 4×10^{-5} , so the uncertainty due to truncation that we

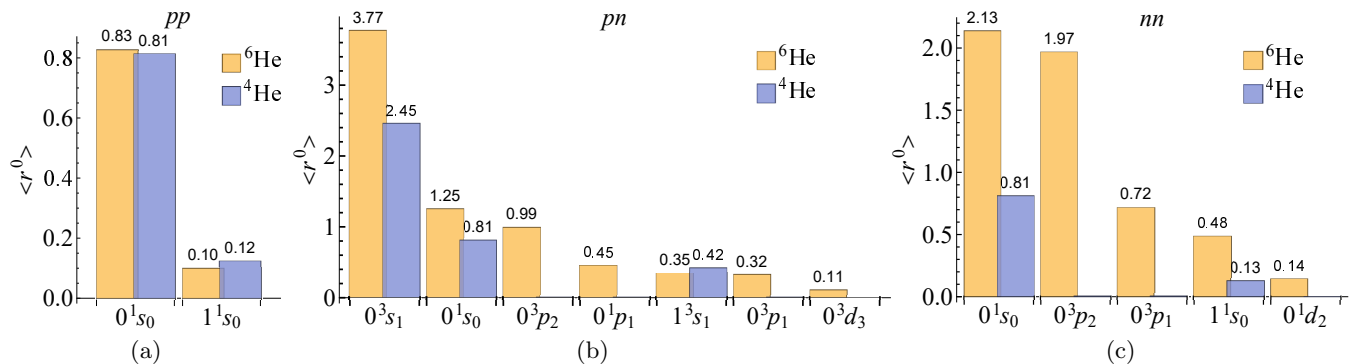


FIG. 4. Major $\langle r^0 \rangle$ two-body contributions of the ground state of ${}^4\text{He}$ and ${}^6\text{He}$ with $N_{\text{max}} = 16$ and $\hbar\Omega = 10$ MeV, for pp (a), pn (b) and nn (c) pairs according to the HO state of relative motion. The bins are arranged by decreasing magnitude for ${}^6\text{He}$, with the corresponding ${}^4\text{He}$ bins shown alongside for comparison. The states shown above account for more than 90% of $\langle r^0 \rangle$ in each isospin-projected pair configuration.

quote only appears in the last significant decimal digit.

Let us now examine the two-body state contributions to $\langle r^0 \rangle$ (labeled by spectroscopic notation $n^{2S+1}l_J$, where $|l - S| \leq J \leq |l + S|$) in Fig. 4 for the three isospin-projected pair configurations. For the ${}^4\text{He}$ ground state, all the major components come from s -states, as expected from a naive shell model. ${}^4\text{He}$ pp is mostly (81%) in the lowest spin-singlet state, with a small portion (12%) in the $n = 1$ spin-singlet s -state. ${}^6\text{He}$ pp is almost identical to ${}^4\text{He}$. ${}^4\text{He}$ pn spin-triplet states are dominated by the lowest two s -states (96%), while ${}^4\text{He}$ pn spin-singlet state is dominated by the lowest s -state (81%). For ${}^6\text{He}$ pn pairs, we see the rise of p/d -states in both spin-singlet and spin-triplet configurations. The three major p -states contribute 22% and the 0^3d_3 state contributes 1% to the overall $\langle r^0 \rangle$. For nn , we again see the rise of higher states (45% p -states and 2% 0^1d_2) in ${}^6\text{He}$. We note that, for nn , due to the $(-1)^{l+S+T} = -1$ antisymmetry constraint, all allowed p -states are spin-triplets and all allowed s/d -states are spin-singlets. We observe that ${}^6\text{He}$ nn spin-triplets are dominantly in p -states and ${}^6\text{He}$ nn spin-singlets are dominantly in s -states.

To sum up, we conclude that the two ${}^6\text{He}$ valence neutrons dominantly form a singlet spin configuration and are mostly in s -states, from the consideration of preserving the ${}^4\text{He}$ two-body spin configuration inside ${}^6\text{He}$ (suggested by the fact that the proton/neutron occupation probabilities at the $0s_{1/2}$ single-particle state in Fig. 3 and pp two-body spin states in Fig. 4(a) remain almost unchanged from ${}^4\text{He}$ to ${}^6\text{He}$), and from the fairly good consistency between the *ab initio* NCSM calculated $\langle r^0 \rangle$ two-body spin/isospin projections and the naively expected values (Table II). This provides an indicator of halo structure in ${}^6\text{He}$ through the following reasoning. The nn spin-singlet s -states have symmetric spatial wave functions Ψ_{nlm} which have non-zero probability close to the center-of-mass of the pair due to the absence of a centrifugal term in the relative Schrödinger equation, resulting in stronger correlation between the two nucleons compared with spin-triplet states. This seems to support

a “di-neutron” halo at some distance from the center-of-mass of the nucleus. The “cigar”-like configuration is another possibility seen in many calculations but appears not to be the dominant configuration [1, 41, 42].

It can be seen from the above analyses that the *ab initio* NCSM calculated $\langle r^0 \rangle$ two-body spin/isospin projections are useful for speculating about the structure of the ${}^6\text{He}$ ground state. We will show in Sec. IV C that combining $\langle r^0 \rangle$ with $\langle r^2 \rangle$ gives us a more quantitative picture of the structure.

C. The expectation values of the r^2 operator

The expectation values of the r^2 operator for different two-body spin and isospin z -projections $\langle r^2[S, t_{za}, t_{zb}] \rangle$ are presented in Table IV. To normalize $\langle r^2[S, t_{za}, t_{zb}] \rangle$ to its average value for a single pair of nucleons, we define the mean square separation between two nucleons of given $\{S, t_{za}, t_{zb}\}$ as

$$\overline{\langle r^2[S, t_{za}, t_{zb}] \rangle} \equiv \frac{\langle r^2[S, t_{za}, t_{zb}] \rangle}{\langle r^0[S, t_{za}, t_{zb}] \rangle}, \quad (15)$$

and the rms separation between two nucleons of given $\{S, t_{za}, t_{zb}\}$ as

$$\overline{\langle r^2[S, t_{za}, t_{zb}] \rangle}^{1/2} \equiv \sqrt{\frac{\langle r^2[S, t_{za}, t_{zb}] \rangle}{\langle r^0[S, t_{za}, t_{zb}] \rangle}}. \quad (16)$$

These derived quantities are shown in the last two columns for each nucleus in Table IV.

These results can be interpreted with the following considerations. Using again the overall antisymmetrization property of fermion pairs as mentioned in Sec. IV B, the rms separation for spin-singlet is expected to be smaller than that for spin-triplet for the pp and nn pairs in their lowest partial waves. This turns out to be true for both ${}^4\text{He}$ (2.5 fm versus 3.1 fm) and ${}^6\text{He}$ (2.6 fm versus 3.3 fm for pp ; 3.7 fm versus 4.5 fm for nn) in Table IV. For pn

TABLE IV. $\langle r^2[S, t_{za}, t_{zb}] \rangle$ [fm²] with five significant digits (digits after the significant digits are grayed out). We also present the mean square separation $\overline{\langle r^2[S, t_{za}, t_{zb}] \rangle}$ [fm²] and the rms separation $\overline{\langle r^2[S, t_{za}, t_{zb}] \rangle}^{1/2}$ [fm] for each nucleus.

		⁴ He			⁶ He		
S		$\langle r^2 \rangle$	$\overline{\langle r^2 \rangle}$	$\overline{\langle r^2 \rangle}^{1/2}$	$\langle r^2 \rangle$	$\overline{\langle r^2 \rangle}$	$\overline{\langle r^2 \rangle}^{1/2}$
<i>pp</i>	0	5.95862	6.10032	2.46988	6.63201	6.85424	2.61806
<i>pp</i>	1	0.22754	9.79581	3.12983	0.36145	11.1484	3.33892
<i>pn</i>	0	5.94563	6.07248	2.46424	24.5046	12.3921	3.52024
<i>pn</i>	1	18.3172	6.06352	2.46242	73.2384	12.1607	3.48721
<i>nn</i>	0	5.89396	6.03411	2.45644	38.7177	13.5121	3.67588
<i>nn</i>	1	0.22648	9.75110	3.12268	63.2643	20.1827	4.49252

pairs, since the two-body isospin T can be either 0 or 1, the spatial part of the wave function for given S can be either symmetric or antisymmetric. Thus, the rms separations for spin-singlet pn pairs and spin-triplet pn pairs are similar (2.46 fm versus 2.46 fm for ⁴He; 3.52 fm versus 3.49 fm for ⁶He).

Comparing ⁶He with ⁴He, we see that the rms separation for the dominant pp spin-singlet configuration, is expanded by 6% from ⁴He to ⁶He. Interestingly, the remaining $\sim 3\%$ (Table II) portion of pp spin-triplet states also experiences a similar expansion in rms separation from ⁴He to ⁶He. On the other hand, the rms separations for nn and pn pairs are expanded by 40%~50% from ⁴He to ⁶He.

Summing over S in both the denominator and numerator of Eq. (15), we define the mean square separation for two nucleons of given $\{t_{za}, t_{zb}\}$ as

$$\overline{\langle r^2[t_{za}, t_{zb}] \rangle} \equiv \frac{\sum_S \langle r^2[S, t_{za}, t_{zb}] \rangle}{\sum_S \langle r^0[S, t_{za}, t_{zb}] \rangle} = \frac{\langle r^2[t_{za}, t_{zb}] \rangle}{\langle r^0[t_{za}, t_{zb}] \rangle}. \quad (17)$$

⁴He and ⁶He have only one pp pair, therefore $\langle r^0[1/2, 1/2] \rangle_{4\text{He}, 6\text{He}} = 1$. Similarly, it is straightforward to note that $\langle r^0[-1/2, 1/2] \rangle_{4\text{He}} = 4$, $\langle r^0[-1/2, 1/2] \rangle_{6\text{He}} = 8$, $\langle r^0[-1/2, -1/2] \rangle_{4\text{He}} = 1$ and $\langle r^0[-1/2, -1/2] \rangle_{6\text{He}} = 6$. The rms separation of given $\{t_{za}, t_{zb}\}$ can be defined as the square root of $\overline{\langle r^2[t_{za}, t_{zb}] \rangle}$. The calculated mean square separations along with the rms separations are shown in Table V. We compare with the corresponding results computed using NNLO_{opt} nucleon-nucleon interaction [43] with $N_{\text{max}} = 14$ in Ref. [44] and find overall consistency.

To characterize a nucleus by an overall nucleon-nucleon separation without specifying nucleon species, we define the mean square separation between two nucleons in a nucleus as

$$\overline{\langle r^2 \rangle} \equiv \frac{\sum_{S, t_{za} \leq t_{zb}} \langle r^2[S, t_{za}, t_{zb}] \rangle}{\sum_{S, t_{za} \leq t_{zb}} \langle r^0[S, t_{za}, t_{zb}] \rangle} = \frac{\langle r^2 \rangle}{A(A-1)/2}, \quad (18)$$

where $A(A-1)/2 = 6$ for ⁴He and $A(A-1)/2 = 15$ for ⁶He. Then the inter-nucleon rms separation is the square root of $\overline{\langle r^2 \rangle}$. From Table IV and Eq. (18), $\overline{\langle r^2 \rangle}_{4\text{He}} = 6.0949$ fm² and $\overline{\langle r^2 \rangle}_{6\text{He}} = 13.781$ fm², which yield $\overline{\langle r^2 \rangle}_{4\text{He}}^{1/2} = 2.4688$ fm and $\overline{\langle r^2 \rangle}_{6\text{He}}^{1/2} = 3.7123$ fm, meaning that the nucleon-nucleon separations in ⁶He, on average, are 50% larger than those in ⁴He.

In summary, the classical structure of ⁴He is a tetrahedron, analyzed from combining rms radii with rms separations. From Table I, the calculated point-proton and point-neutron rms radii for ⁴He are nearly identical, around $r_0 = 1.51$ fm. And from Table V, ⁴He pp , pn and nn rms separations are also very similar, about $a = 2.47$ fm. The ratio $a/r_0 = 1.636$ is approximately the same as the side length to the center-to-vertex distance ratio of a tetrahedron $2\sqrt{6}/3 = 1.633$. This suggests a route by which we can relate our quantum many-body results to a classical picture that depicts ⁴He as a tetrahedron with protons and neutrons at the tetrahedron's vertices.

To analyze the structure of ⁶He, we notice a 6.3% increase in pp rms separation from ⁴He to ⁶He (Table V), representing a substantially weaker effect than the corresponding 25% increase in r_p (Table I). This means that not only does the “ α core” swell, but also the center of mass of ⁶He is no longer centered at the center of the “ α core”. The center of mass is likely to have longer distances from the two protons in ⁶He, compared with ⁴He. Meanwhile, pn (nn) rms separation of ⁶He increases by 41.9% (66.6%), compared with that of ⁴He. Since pn and nn contain more than one pair of nucleons, a binary model is constructed to capture the main features of these changes. We introduce x (y) as the ratio between the rms separation of pn^α or $n^\alpha n^\alpha$ (pn^h , $n^\alpha n^h$ or $n^h n^h$) in ⁶He and the rms separation of pn or nn in ⁴He, i.e.,

$$\frac{r_{pn/nn}^{(6\text{He})}}{r_{pn/nn}^{(4\text{He})}} = \begin{cases} x, & \text{both } ^6\text{He} \text{ nucleons within the “}\alpha \text{ core”} \\ y, & \text{otherwise} \end{cases}. \quad (19)$$

Matching the percentage increases,

$$\frac{r_{pn}^{(6\text{He})} - r_{pn}^{(4\text{He})}}{r_{pn}^{(4\text{He})}} = \sqrt{\frac{4x^2 + 4y^2}{8}} - 1 = 41.9\%, \quad (20)$$

and

$$\frac{r_{nn}^{(6\text{He})} - r_{nn}^{(4\text{He})}}{r_{nn}^{(4\text{He})}} = \sqrt{\frac{x^2 + 5y^2}{6}} - 1 = 66.6\%. \quad (21)$$

Solving these two equations yields $x = 0.93$ and $y = 1.78$. This suggests that the pn/nn rms separation within the “ α core” stays nearly the same as for ⁴He ($x \approx 1$), while the rms separation of two nucleons with correlation extending outside of the “ α core” is found to increase by almost 80%, supporting the formation of a halo.

TABLE V. $\langle r^2[t_{za}, t_{zb}] \rangle$ [fm²] computed from Table IV, together with the mean square separation $\overline{\langle r^2[t_{za}, t_{zb}] \rangle}$ [fm²] and the nucleon-nucleon rms separation $\overline{\langle r^2[t_{za}, t_{zb}] \rangle}^{1/2}$ [fm]. Digits after the five significant digits are grayed out. We compare our rms separations with those of Ref. [44].

	⁴ He				⁶ He			
	$\langle r^2 \rangle$	$\overline{\langle r^2 \rangle}$	$\overline{\langle r^2 \rangle}^{1/2}$	[44]	$\langle r^2 \rangle$	$\overline{\langle r^2 \rangle}$	$\overline{\langle r^2 \rangle}^{1/2}$	[44]
<i>pp</i>	6.18616	6.18616	2.48720	2.40	6.99346	6.99346	2.64452	2.62
<i>pn</i>	24.2629	6.06572	2.46287	2.40	97.7429	12.2179	3.49541	3.3
<i>nn</i>	6.12044	6.12044	2.47395	2.40	101.982	16.9970	4.12274	3.9

V. CONCLUSION

We show that the formation of the halo structure of ⁶He can be examined from the coordinate-space two-body correlation operators r^0 and r^2 using the *ab initio* NCSM with the Daejeon16 plus Coulomb interactions.

We examine the dominant two-body spin configurations of ⁴He and ⁶He by analyzing the results of r^0 projected on two-body spin and isospin z -components. Combined with the analysis of the single-particle states and the two-body states of the ground state of ⁴He and ⁶He, the two valence neutrons of ⁶He predominantly form a spin-singlet configuration where symmetry regarding the probability of forming an arbitrary two-body spin is largely respected. We demonstrate that the inclusion of results for expectation values of r^2 provides a more subtle picture of ⁴He and ⁶He via the geometrical relations among the calculated point-nucleon rms radii and the inter-nucleon rms separations. We utilize a binary model to describe the inter-nucleon separations of ⁶He. We conclude that ⁴He’s classical structure is essentially a tetrahedron, and the inter-nucleon rms separation within the “ α core” of ⁶He is comparable to that of ⁴He. On the other hand, the rms separation between the core nucleons and the halo neutrons of ⁶He is about 80% larger than the above scale. We observe the signature of a moderately swollen ⁶He “ α core” through the 6.3% increase in rms separation between the two protons compared to ⁴He. Since this cannot explain the 25% increase in the point-proton radius r_p of ⁶He relative to ⁴He, we conclude that the primary effect responsible for the r_p increase comes from the “ α core” deviating from the center of mass of ⁶He, which is also supported by our calculated proton-neutron and neutron-neutron rms separations. In the future, we are also interested in exploring other spatial correlation operators, such as r^4 and r^6 , to provide a richer physical picture of the structure of light nuclei, constructing semi-classical models capable of presenting detailed structural information of a nucleus, and improving the extrapolation techniques for the long-range operators that are used to compute spatial observables.

ACKNOWLEDGMENTS

We wish to acknowledge useful discussions with Pieter Maris and Mark Caprio. This work was supported in part by the US Department of Energy (DOE) under Grant Nos. DE-FG02-87ER40371, DE-SC0018223 (SciDAC-4/NUCLEI), DE-SC0023495 (SciDAC-5/NUCLEI), DE-SC0023707 (Quantum Horizons – NuHaQ) and DE-FG02-95ER40934. This work was performed under the auspices of the U.S. Department of Energy by Lawrence Livermore National Laboratory under Contract DE-AC52-07NA27344. Computational resources were provided by the National Energy Research Scientific Computing Center (NERSC), which is supported by the US DOE Office of Science under Contract No. DE-AC02-05CH11231 using NERSC award NP-ERCAP0020944. Tobias Frederico thanks the hospitality of the Department of Physics and Astronomy of the Iowa State University and to the Fulbright Brazil for the financial support during his visits on 2018 and 2019. TF also thanks the National Council for Scientific and Technological Development (CNPq) Grant No. 306834/2022-7, the São Paulo Research Foundation (FAPESP) Grant Nos. 2023/13749-1 and 2024/17816-8, and the INCT-FNA project 408419/2024-5. Peng Yin is supported by Natural Science Foundation of Henan under Grant No. 252300421486.

Appendix A: Rotationally invariant operator with given two-body spin and given pair of isospin z -projections

We consider matrix elements of local two-body operators of the form $O(r)P_S$, that is, a rotationally invariant (scalar) operator depending only on the relative spatial coordinate r of the two nucleons, in combination with the two-body spin projection operator P_S , where $\langle S_1 | P_S | S_2 \rangle = \delta_{S_1 S_2}$. We adopt the shorthand $\mathcal{O}(r)[S] \equiv O(r)P_S$, and below we will focus on operators $\mathcal{O}(r)[S, t_{za}, t_{zb}]$ which also project on given isospin z -components t_{za} and t_{zb} of the two nucleons.

Since the $O(r)$ operator is a rank-0 tensor, from the Wigner-Eckart theorem, $\langle \alpha\beta; J' M' | O(r) | \gamma\delta; JM \rangle = \delta_{J' J} \delta_{M' M} \langle \alpha\beta; J || O(r) || \gamma\delta; J \rangle$, where, in our convention,

the double-bar (reduced) matrix element does not factor out $(2J+1)^{-\frac{1}{2}}$ and remains consistent with the Wigner-Eckart theorem formulated in Eq. (4.15) of Ref. [45].

In order to select the states of given two-body spin, one can resolve quantities in terms of two-body spin S ($\vec{S} = \vec{s}_\alpha + \vec{s}_\beta$) and two-body total orbital angular momentum

L ($\vec{L} = \vec{l}_\alpha + \vec{l}_\beta$) by inserting

$$\mathbb{1} = \sum_{LS} |n_\alpha l_\alpha n_\beta l_\beta L, \frac{1}{2} \frac{1}{2} S; J\rangle \langle n_\alpha l_\alpha n_\beta l_\beta L, \frac{1}{2} \frac{1}{2} S; J| \quad (\text{A1})$$

into $\langle \alpha\beta; J || O(r) || \gamma\delta; J \rangle$ twice, where the spin quantum numbers ($\frac{1}{2}$) are explicit while the isospin quantum numbers are omitted for simplification of the notation.

We find that the reduced matrix element of $\mathcal{O}(r)[S]$ can be expressed as

$$\begin{aligned} & \langle \alpha\beta; J || \mathcal{O}(r)[S] || \gamma\delta; J \rangle \\ &= \sum_{L_1 L_2 S_1 S_2} \langle \alpha\beta; J | n_\alpha l_\alpha n_\beta l_\beta L_1, \frac{1}{2} \frac{1}{2} S_1; J \rangle \langle n_\alpha l_\alpha n_\beta l_\beta L_1, \frac{1}{2} \frac{1}{2} S_1; J || O(r) || n_\gamma l_\gamma n_\delta l_\delta L_2, \frac{1}{2} \frac{1}{2} S_2; J \rangle \langle n_\gamma l_\gamma n_\delta l_\delta L_2, \frac{1}{2} \frac{1}{2} S_2; J | \gamma\delta; J \rangle \\ & \quad \times \delta_{S S_1} \delta_{S_1 S_2} \\ &= \sum_L \langle n_\alpha l_\alpha n_\beta l_\beta L || O(r) || n_\gamma l_\gamma n_\delta l_\delta L \rangle \langle \alpha\beta; J | n_\alpha l_\alpha n_\beta l_\beta L, \frac{1}{2} \frac{1}{2} S; J \rangle \langle n_\gamma l_\gamma n_\delta l_\delta L, \frac{1}{2} \frac{1}{2} S; J | \gamma\delta; J \rangle, \end{aligned} \quad (\text{A2})$$

where in the last line we have used the fact that $O(r)$ is rotationally invariant, so L is invariant upon the action of $O(r)$, i.e., $\langle L_1 | O(r) | L_2 \rangle = \langle L_1 | O(r) \delta_{L_1 L_2} | L_2 \rangle$. We now drop the subscript of L for notational simplicity. There is no need to label J values in the reduced matrix elements, because $O(r)$ only produces a dependence on the radial and orbital quantum numbers.

We identify the “ $LS - jj$ ” coupling coefficient [25, 46], i.e., the transformation coefficient between Russell-Saunders coupling and the spin-orbit coupling in

Eq. (A2), by first expanding the notation

$$\begin{aligned} & \langle \alpha\beta; J | n_\alpha l_\alpha n_\beta l_\beta L, \frac{1}{2} \frac{1}{2} S; J \rangle \\ &= \langle n_\alpha l_\alpha \frac{1}{2} j_\alpha, n_\beta l_\beta \frac{1}{2} j_\beta; J | n_\alpha l_\alpha n_\beta l_\beta L, \frac{1}{2} \frac{1}{2} S; J \rangle \\ &= \langle l_\alpha \frac{1}{2} j_\alpha, l_\beta \frac{1}{2} j_\beta; J | l_\alpha l_\beta L, \frac{1}{2} \frac{1}{2} S; J \rangle \\ &= \sqrt{(2j_\alpha + 1)(2j_\beta + 1)(2L + 1)(2S + 1)} \left\{ \begin{matrix} l_\alpha & l_\beta & L \\ 1/2 & 1/2 & S \\ j_\alpha & j_\beta & J \end{matrix} \right\}, \end{aligned} \quad (\text{A3})$$

where the curly brackets represent the $9j$ symbols, which is another way to write an assembly of Clebsch-Gordan coefficients.

One then obtains

$$\begin{aligned} \langle \alpha\beta; J || \mathcal{O}(r)[S] || \gamma\delta; J \rangle &= \langle n_\alpha l_\alpha n_\beta l_\beta L || O(r) || n_\gamma l_\gamma n_\delta l_\delta L \rangle \\ & \quad \times (2S + 1) \sqrt{(2j_\alpha + 1)(2j_\beta + 1)(2j_\gamma + 1)(2j_\delta + 1)} \sum_L (2L + 1) \left\{ \begin{matrix} l_\alpha & l_\beta & L \\ 1/2 & 1/2 & S \\ j_\alpha & j_\beta & J \end{matrix} \right\} \left\{ \begin{matrix} l_\gamma & l_\delta & L \\ 1/2 & 1/2 & S \\ j_\gamma & j_\delta & J \end{matrix} \right\}. \end{aligned} \quad (\text{A4})$$

To project this two-body operator on a fixed pair of isospin z -components, we define $\mathcal{O}(r)[S, t_{za}, t_{zb}] = O(r) P_S P_{t_{za}, t_{zb}}$, with

$$\begin{aligned} \langle \alpha\beta; J || \mathcal{O}(r)[S, t_{za}, t_{zb}] || \gamma\delta; J \rangle &= \langle \alpha\beta; J || \mathcal{O}(r)[S, t_{za}, t_{zb}] \delta_{t_{z\alpha}, t_{z\gamma}} \delta_{t_{z\beta}, t_{z\delta}} || \gamma\delta; J \rangle \\ &= \langle \alpha\beta; J || \mathcal{O}(r)[S] || \gamma\delta; J \rangle \delta_{t_{z\alpha}, t_{z\gamma}} \delta_{t_{z\beta}, t_{z\delta}} g(t_{z\alpha}, t_{z\beta})_{t_{za} \leq t_{zb}}. \end{aligned} \quad (\text{A5})$$

The resulting matrix element becomes

$$\begin{aligned}
\langle \alpha\beta; J'M' | \mathcal{O}(r) [S, t_{za}, t_{zb}] | \gamma\delta; JM \rangle &= \delta_{t_{z\alpha}, t_{z\gamma}} \delta_{t_{z\beta}, t_{z\delta}} \delta_{J'J} \delta_{M'M} g(t_{z\alpha}, t_{z\beta})_{t_{za} \leq t_{zb}} \\
&\times (2S+1) \sqrt{(2j_\alpha+1)(2j_\beta+1)(2j_\gamma+1)(2j_\delta+1)} \\
&\times \sum_L (2L+1) \begin{Bmatrix} l_\alpha & l_\beta & L \\ 1/2 & 1/2 & S \\ j_\alpha & j_\beta & J \end{Bmatrix} \begin{Bmatrix} l_\gamma & l_\delta & L \\ 1/2 & 1/2 & S \\ j_\gamma & j_\delta & J \end{Bmatrix} \langle n_\alpha l_\alpha n_\beta l_\beta L | \mathcal{O}(r) | n_\gamma l_\gamma n_\delta l_\delta L \rangle.
\end{aligned} \tag{A6}$$

Appendix B: Harmonic oscillator matrix elements

One can obtain the matrix elements of operators $O(r) = r^0$ and $O(r) = r^2$ in the convenient HO basis with the knowledge that the angular parts of the wavefunctions are not affected, so only matrix elements with $l = l'$ are non-zero:

$$\langle n'l' | r^0 | nl \rangle = \delta_{n,n'} \delta_{l,l'}, \tag{B1}$$

$$\begin{aligned}
&\langle n'l' | r^2 | nl \rangle \\
&= b^2 \left[\left(2n+l + \frac{3}{2} \right) \delta_{n,n'} - \sqrt{n(n+l + \frac{1}{2})} \delta_{n,n'+1} \right. \\
&\quad \left. - \sqrt{(n+1)(n+l + \frac{3}{2})} \delta_{n,n'-1} \right] \delta_{l,l'},
\end{aligned} \tag{B2}$$

where $b \equiv \sqrt{\hbar/(\mu\Omega)}$ with the reduced mass $\mu = m_N/2$ ($m_N = 938.92 \text{ MeV}/c^2$ is the average mass of a neutron and a proton with their mass given by PDG [36]). The derivation of these matrix elements has been detailed in the Appendix of Ref. [47].

Appendix C: Moshinsky transformation

We follow the Moshinsky transformation as discussed in Ref. [48]. The single-particle HO wave function in the two-body relative frame is

$$\langle \vec{r} | nlm \rangle. \tag{C1}$$

The two-body oscillator wave function with two-body total orbital angular momentum L and its projection λ reads

$$\begin{aligned}
&\langle \vec{r}_1 \vec{r}_2 | n_1 l_1 n_2 l_2 L \lambda \rangle \\
&= R_{n_1 l_1}(r_1) R_{n_2 l_2}(r_2) \sum_{m_1 m_2} C_{m_1 l_1 m_2 l_2}^L Y_{l_1 m_1}(\mathbf{\Omega}_1) Y_{l_2 m_2}(\mathbf{\Omega}_2).
\end{aligned} \tag{C2}$$

Noting that the two-body relative coordinates

$$\vec{r} = \frac{1}{\sqrt{2}}(\vec{r}_1 - \vec{r}_2), \quad \vec{R} = \frac{1}{\sqrt{2}}(\vec{r}_1 + \vec{r}_2) \tag{C3}$$

and introducing the two-body center-of-mass orbital angular momentum \mathcal{L} and its projection \mathcal{M} , and the center-of-mass radial quantum number \mathcal{N} , one arrives at

$$\begin{aligned}
\langle \vec{r} \vec{R} | n_1 l_1 n_2 l_2 L \lambda \rangle &= \sum_{i\mathcal{L}} \psi_i(r, R) \\
&\times \sum_{m\mathcal{M}} C_m^l \mathcal{C}_\mathcal{M}^L Y_{lm}(\mathbf{\Omega}_r) Y_{\mathcal{L}\mathcal{M}}(\mathbf{\Omega}_R),
\end{aligned} \tag{C4}$$

where $i \equiv \{n_1 l_1 n_2 l_2 l \mathcal{L} L\}$, and

$$\psi_i(r, R) = \sum_{n\mathcal{N}} \langle nl, \mathcal{N}\mathcal{L}; L | n_1 l_1, n_2 l_2; L \rangle_1 R_{ni}(r) R_{\mathcal{N}\mathcal{L}}(R), \tag{C5}$$

with the well-known Moshinsky brackets $\langle nl, \mathcal{N}\mathcal{L}; L | n_1 l_1, n_2 l_2; L \rangle_1$ subscripted by the ratio of the mass of the two bodies (see e.g., Ref. [49]).

-
- [1] M. V. Zhukov, B. V. Danilin, D. V. Fedorov, J. M. Bang, I. J. Thompson, and J. S. Vaagen, Bound state properties of Borromean halo nuclei: ${}^6\text{He}$ and ${}^{11}\text{Li}$, *Physics Reports* **231**, 151 (1993).
 - [2] P. G. Hansen, A. S. Jensen, and B. Jonson, Nuclear halos, *Annual review of nuclear and particle science* **45**, 591 (1995).
 - [3] A. S. Jensen, K. Riisager, D. V. Fedorov, and E. Garrido, Structure and reactions of quantum halos, *Rev. Mod. Phys.* **76**, 215 (2004).
 - [4] B. Jonson, Light dripline nuclei, *AIP Conference Proceedings* **495**, 3 (1999).
 - [5] K. Riisager, Halos and related structures, *Physica Scripta* **T152**, 014001 (2013).
 - [6] I. Tanihata, H. Hamagaki, O. Hashimoto, Y. Shida, N. Yoshikawa, K. Sugimoto, O. Yamakawa, T. Kobayashi, and N. Takahashi, Measurements of interaction cross sections and nuclear radii in the light p -shell region, *Phys. Rev. Lett.* **55**, 2676 (1985).
 - [7] I. Tanihata, Neutron halo nuclei, *Journal of Physics G:*

Nuclear and Particle Physics **22**, 157 (1996).

- [8] I. Tanihata, Nuclear physics with RIB's: How it all started, *The European Physical Journal Plus* **131**, 90 (2016).
- [9] T. Kobayashi, O. Yamakawa, K. Omata, K. Sugimoto, T. Shimoda, N. Takahashi, and I. Tanihata, Projectile fragmentation of the extremely neutron-rich nucleus ^{11}Li at 0.79 GeV/nucleon, *Phys. Rev. Lett.* **60**, 2599 (1988).
- [10] N. A. Orr, N. Anantaraman, S. M. Austin, C. A. Bertulani, K. Hanold, J. H. Kelley, D. J. Morrissey, B. M. Sherrill, G. A. Souliotis, M. Thoennessen, J. S. Winfield, and J. A. Winger, Momentum distributions of ^9Li fragments following the breakup of ^{11}Li , *Phys. Rev. Lett.* **69**, 2050 (1992).
- [11] T. Nakamura, A. M. Vinodkumar, T. Sugimoto, N. Aoi, H. Baba, D. Bazin, N. Fukuda, T. Gomi, H. Hasegawa, N. Imai, M. Ishihara, T. Kobayashi, Y. Kondo, T. Kubo, M. Miura, T. Motobayashi, H. Otsu, A. Saito, H. Sakurai, S. Shimoura, K. Watanabe, Y. X. Watanabe, T. Yakushiji, Y. Yanagisawa, and K. Yoneda, Observation of strong low-lying $E1$ strength in the two-neutron halo nucleus ^{11}Li , *Phys. Rev. Lett.* **96**, 252502 (2006).
- [12] T. Aumann, D. Aleksandrov, L. Axelsson, T. Baumann, M. J. G. Borge, L. V. Chulkov, J. Cub, W. Dostal, B. Eberlein, T. W. Elze, H. Emling, H. Geissel, V. Z. Goldberg, M. Golovkov, A. Grünschloß, M. Hellström, K. Hencken, J. Holeczek, R. Holzmann, B. Jonson, A. A. Korshenninikov, J. V. Kratz, G. Kraus, R. Kulesa, Y. Leifels, A. Leistenschneider, T. Leth, I. Mukha, G. Münzenberg, F. Nickel, T. Nilsson, G. Nyman, B. Petersen, M. Pfützner, A. Richter, K. Riisager, C. Scheidenberger, G. Schrieder, W. Schwab, H. Simon, M. H. Smedberg, M. Steiner, J. Stroth, A. Surowiec, T. Suzuki, O. Tengblad, and M. V. Zhukov, Continuum excitations in ^6He , *Phys. Rev. C* **59**, 1252 (1999).
- [13] N. Fukuda, T. Nakamura, N. Aoi, N. Imai, M. Ishihara, T. Kobayashi, H. Iwasaki, T. Kubo, A. Mengoni, M. Notani, H. Otsu, H. Sakurai, S. Shimoura, T. Teranishi, Y. X. Watanabe, and K. Yoneda, Coulomb and nuclear breakup of a halo nucleus ^{11}Be , *Phys. Rev. C* **70**, 054606 (2004).
- [14] C. Romero-Redondo, P. Navrátil, S. Quaglioni, and G. Hupin, *Ab initio* NCSM/RGM for three-body cluster systems and application to $^4\text{He} + n + n$, *Few-Body Systems* **55**, 927 (2014).
- [15] S. Quaglioni, P. Navrátil, G. Hupin, J. Langhammer, C. Romero-Redondo, and R. Roth, No-core shell model analysis of light nuclei, *Few-Body Systems* **54**, 877 (2013).
- [16] C. Romero-Redondo, S. Quaglioni, P. Navrátil, and G. Hupin, $^4\text{He} + n + n$ continuum within an *ab initio* framework, *Phys. Rev. Lett.* **113**, 032503 (2014).
- [17] P. Navrátil, Cluster form factor calculation in the *ab initio* no-core shell model, *Phys. Rev. C* **70**, 054324 (2004).
- [18] S. Quaglioni, C. Romero-Redondo, P. Navrátil, and G. Hupin, Three-cluster dynamics within the *ab initio* no-core shell model with continuum: How many-body correlations and α clustering shape ^6He , *Phys. Rev. C* **97**, 034332 (2018).
- [19] E. Epelbaum, H. Krebs, T. A. Lähde, D. Lee, and U.-G. Meißner, Structure and rotations of the Hoyle state, *Phys. Rev. Lett.* **109**, 252501 (2012).
- [20] T. Otsuka, T. Abe, T. Yoshida, Y. Tsunoda, N. Shimizu, N. Itagaki, Y. Utsuno, J. Vary, P. Maris, and H. Ueno, α -Clustering in atomic nuclei from first principles with statistical learning and the Hoyle state character, *Nature Communications* **13**, 2234 (2022).
- [21] C. Robin, M. J. Savage, and N. Pillet, Entanglement rearrangement in self-consistent nuclear structure calculations, *Phys. Rev. C* **103**, 034325 (2021).
- [22] B. R. Barrett, P. Navrátil, and J. P. Vary, *Ab initio* no core shell model, *Progress in Particle and Nuclear Physics* **69**, 131 (2013).
- [23] C. Cockrell, J. P. Vary, and P. Maris, Lithium isotopes within the *ab initio* no-core full configuration approach, *Phys. Rev. C* **86**, 034325 (2012).
- [24] C. Cockrell, *Ab initio nuclear structure calculations for light nuclei (2012)*, Ph.D. thesis, Iowa State University (2012).
- [25] A. R. Edmonds, *Angular Momentum in Quantum Mechanics* (Princeton University Press, 2016).
- [26] M. A. Caprio, A. E. McCoy, and P. J. Fasano, Intrinsic operators for the translationally-invariant many-body problem, *Journal of Physics G: Nuclear and Particle Physics* **47**, 122001 (2020).
- [27] M. A. Caprio, P. Maris, and J. P. Vary, Halo nuclei ^6He and ^8He with the Coulomb-Sturmian basis, *Phys. Rev. C* **90**, 034305 (2014).
- [28] A. Shirokov, I. Shin, Y. Kim, M. Sosonkina, P. Maris, and J. Vary, N3LO NN interaction adjusted to light nuclei in *ab exitu* approach, *Physics Letters B* **761**, 87 (2016).
- [29] P. Maris, M. Sosonkina, J. P. Vary, E. Ng, and C. Yang, Scaling of *ab-initio* nuclear physics calculations on multi-core computer architectures, *Procedia Computer Science (ICCS 2010)* **1**, 97 (2010).
- [30] H. M. Aktulga, C. Yang, E. G. Ng, P. Maris, and J. P. Vary, Improving the scalability of a symmetric iterative eigensolver for multi-core platforms, *Concurrency and Computation: Practice and Experience* **26**, 2631 (2014).
- [31] F. Wegner, Flow-equations for Hamiltonians, *Annalen der Physik* **506**, 77 (1994).
- [32] S. D. Glazek and K. G. Wilson, Perturbative renormalization group for Hamiltonians, *Phys. Rev. D* **49**, 4214 (1994).
- [33] Z.-T. Lu, P. Mueller, G. W. F. Drake, W. Nörtershäuser, S. C. Pieper, and Z.-C. Yan, Colloquium: Laser probing of neutron-rich nuclei in light atoms, *Rev. Mod. Phys.* **85**, 1383 (2013).
- [34] I. Sick, Precise root-mean-square radius of ^4He , *Phys. Rev. C* **77**, 041302 (2008).
- [35] M. Brodeur, T. Brunner, C. Champagne, S. Ettenauer, M. J. Smith, A. Lapierre, R. Ringle, V. L. Ryjkov, S. Bacca, P. Delheij, G. W. F. Drake, D. Lunney, A. Schwenk, and J. Dilling, First direct mass measurement of the two-neutron halo nucleus ^6He and improved mass for the four-neutron halo ^8He , *Phys. Rev. Lett.* **108**, 052504 (2012).
- [36] P. A. Zyla et al. (Particle Data Group), The review of particle physics, *Prog. Theor. Exp. Phys.* **2020**, 083C01 (2020).
- [37] A. Ong, J. C. Berengut, and V. V. Flambaum, Effect of spin-orbit nuclear charge density corrections due to the anomalous magnetic moment on halonuclei, *Phys. Rev. C* **82**, 014320 (2010).
- [38] P. J. Mohr, D. B. Newell, B. N. Taylor, and E. Tiesinga, Codata recommended values of the fundamental physical constants: 2022, *Rev. Mod. Phys.* **97**, 025002 (2025).
- [39] D. M. Rodkin and Y. M. Tchuvil'sky, Two-dimensional

- extrapolation procedure for an ab initio study of nuclear size parameters and the properties of the halo nucleus ${}^6\text{He}$, *Phys. Rev. C* **106**, 034305 (2022).
- [40] P. Cappellaro, Chapter 5. Nuclear Structure, in *22.02 Introduction to Applied Nuclear Physics. Spring 2012* (MIT OpenCourseWare. License: Creative Commons BY-NC-SA. Massachusetts Institute of Technology, Cambridge, MA, 2012).
- [41] K. Hagino and H. Sagawa, Pairing correlations in nuclei on the neutron-drip line, *Phys. Rev. C* **72**, 044321 (2005).
- [42] G. Papadimitriou, A. T. Kruppa, N. Michel, W. Nazarewicz, M. Płoszajczak, and J. Rotureau, Charge radii and neutron correlations in helium halo nuclei, *Phys. Rev. C* **84**, 051304 (2011).
- [43] A. Ekström, G. Baardsen, C. Forssén, G. Hagen, M. Hjorth-Jensen, G. R. Jansen, R. Machleidt, W. Nazarewicz, T. Papenbrock, J. Sarich, and S. M. Wild, Optimized chiral nucleon-nucleon interaction at next-to-next-to-leading order, *Phys. Rev. Lett.* **110**, 192502 (2013).
- [44] D. Sääf, *Bridging scales in nuclear physics*, Ph.D. thesis, Chalmers University of Technology (2016).
- [45] D. M. Brink and G. R. Satchler, *Angular momentum* (Oxford University Press, USA, 1968).
- [46] E. U. Condon, E. U. Condon, and G. H. Shortley, *The theory of atomic spectra* (Cambridge University Press, 1951).
- [47] R. A. M. Basili, *Nuclear properties with effective operators (2019)*, Ph.D. thesis, Iowa State University (2019).
- [48] M. Znojil, Moshinsky brackets for light nuclei, *Phys. Rev. C* **15**, 423 (1977).
- [49] M. Sotona and M. Gmitro, Generalized transformation brackets for the harmonic oscillator functions, *Computer Physics Communications* **3**, 53 (1972).